

pressure pulses (25 to 40 kPa for 25 to 200 ms) through a "puffer" pipette (2 to 4 μm in tip diameter) placed 40 to 60 μm away from the recorded cell. Muscarinic and nicotinic receptor antagonists, scopolamine (5 mM) and hexamethonium (5 mM), were applied in 30 to 50 μl of ACSF directly into the recording chamber while it was perfused with ACSF at the rate of 1.5 ml/min. Effects of these antagonists usually appeared within 1 to 4 min. Other agents such as 6,7-dinitroquinoxaline-2,3-dione (DNQX, 20 μM) and 3-(2-carboxypiperazin-4-yl)-1-propenyl-1-phosphonic acid (D-CPPene, 5 μM), GABA receptor antagonist, bicuculline (10 μM), as well as tetrodotoxin (TTX, 1 μM), were added to the perfusate and bath applied. To estimate the reversal potential of ACh-induced conductance changes, we plotted the current responses versus ramp voltage in control solution and after drug application and obtained current difference-voltage (ΔI -V) plots by subtracting the control current from ACh current. We estimated the reversal potentials by extrapolating the linear fitting curve to $\Delta I = 0$ or using the crossing points of the ΔI -V curve to the voltage axis at $\Delta I = 0$ (Fig. 3).

11. After the physiological experiments, slices containing biocytin-filled neurons were processed with standard avidin-biotin-peroxidase methods as described elsewhere in detail [K. Horikawa and W. E. Armstrong, *J. Neurosci. Methods* **25**, 1 (1988); G. F. Tseng, I. Parada, D. A. Prince, *ibid.* **37**, 121 (1991)]. Labeled neurons were examined under the light microscope and drawn with a camera lucida, and the axonal arbor representations were exported as bitmap files. Total axonal length per 50- μm horizontal strip was estimated by measuring the integrated bitmap density. Data were then aligned approximately to the middle of the layer V for statistical analysis for which the Mann-Whitney test was used. The results were presented as mean \pm SEM.
12. R. C. Foehring, N. M. Lorenzon, P. Herron, C. J. Wilson, *J. Neurophysiol.* **66**, 1825 (1991).
13. D. A. McCormick, B. W. Connors, J. W. Lighthall, D. A. Prince, *ibid.* **54**, 782 (1985).
14. The differential action of ACh on LTS compared with FS cells remained after synaptic transmission was blocked by perfusing the slice with ACSF containing low Ca^{++} (0.5 mM) and high Mg^{++} (8 mM) [$n = 3$ for LTS cells and $n = 3$ for FS cells; Fig. 2, C (top) and D (top)]; glutamatergic receptor antagonists, DNQX (20 μM) and D-CPPene (5 μM), and the GABA_A receptor antagonist, bicuculline (10 μM) [$n = 2$ for LTS cells and $n = 2$ for FS cells; Fig. 2, C (bottom) and D (bottom)]; or 1 μM TTX ($n = 3$ for LTS and $n = 2$ for FS; Z. Xiang, J. R. Huguenard, D. A. Prince, data not shown).
15. A. U. Larkman, G. Major, K. J. Stratford, J. J. Jack, *J. Comp. Neurol.* **323**, 137 (1992); N. Spruston, D. B. Jaffe, D. Johnston, *Trends. Neurosci.* **17**, 161 (1994).
16. Z. Xiang, I. Parada, J. R. Huguenard, D. A. Prince, *Soc. Neurosci. Abstr.* **23**, 359 (1997).
17. In experiments in which effects of ACh on sIPSCs from layer V pyramidal cells were examined, the extracellular KCl was increased to 10 mM to increase the frequency of spike-driven events, and DNQX (20 μM) and D-CPPene (5 μM) were included in perfusate to block the ionotropic glutamatergic synaptic transmission. Pipette solution contained 65 mM KCl, 65 mM potassium gluconate, 1 mM MgCl_2 , 1 mM CaCl_2 , 10 mM Hepes, 10 mM EGTA, 3 mM ATP, and 0.2 to 0.4 mM GTP. With this pipette solution, calculated chloride equilibrium potential was -15 mV based on the Nernst equation with activity coefficients for extracellular Cl^- of 0.76 and intracellular Cl^- of 0.80 and taking into account the permeability of gluconate through Cl^- channels [J. L. Barker and N. L. Harrison, *J. Physiol.* **403**, 41 (1988)]. In such a recording condition, sIPSCs were inward currents at a holding potential of -70 mV. ACh were locally applied as described in (10). Kolmogorov-Smirnov (K-S) statistics were used to analyze the sIPSC data.
18. In one pyramidal cell, ACh application gave rise to an increase in frequency of large, slow events. This cell showed an increase in sIPSC rise time after ACh application similar to that seen in six other neurons. We speculate that the large-amplitude sIPSCs in this particular case may have reflected an unusually large

- number of synaptic contacts from one or more LTS cells onto the pyramidal neuron.
19. D. A. McCormick and D. A. Prince, *J. Neurosci.* **7**, 742 (1987); L. J. Reece and P. A. Schwartzkroin, *Brain Res.* **540**, 287 (1991); A. R. McQuiston and D. V. Madison, *Soc. Neurosci. Abstr.* **23**, 2009 (1997); C. J. Frazier et al., *J. Neurosci.* **18**, 1187 (1998); M. Alkondon, E. F. Pereira, C. T. Barbosa, E. X. Albuquerque, *J. Pharmacol. Exp. Ther.* **283**, 1396 (1997).
20. K. H. Lee and D. A. McCormick, *J. Neurophysiol.* **73**, 2123 (1995).
21. A. R. McQuiston and D. V. Madison, *Soc. Neurosci. Abstr.* **22**, 786 (1996).
22. D. A. McCormick and D. A. Prince, *Nature* **319**, 402 (1986); D. A. McCormick and H. C. Pape, *ibid.* **334**, 246 (1988).
23. D. A. McCormick and D. A. Prince, *Proc. Natl. Acad. Sci. U.S.A.* **82**, 6344 (1985).

24. ———, *J. Physiol.* **375**, 169 (1986).
25. Y. Kawaguchi, *J. Neurophysiol.* **78**, 1743 (1997).
26. L. J. Reece and P. A. Schwartzkroin, *Brain Res.* **566**, 115 (1991); T. A. Pittler and B. E. Alger, *J. Physiol.* **450**, 127 (1992).
27. J. W. Phillis and D. H. York, *Brain Res.* **10**, 297 (1968); K. Krnjević, *Physiol. Rev.* **54**, 418 (1974).
28. D. A. Prince and B. J. Wilder, *Arch. Neurol.* **16**, 194 (1967).
29. We thank I. Parada for her excellent assistance during the course of the experiments. The work was supported by NIH grants NS 12151, NS 07280, NS 06477, and NS 10474 from the National Institute of Neurological Disorders and Stroke and the Morris and Pimley research funds.

7 April 1998; accepted 8 July 1998

Neural Crest Specification Regulated by the Helix-Loop-Helix Repressor Id2

Brad J. Martinsen and Marianne Bronner-Fraser*

Vertebrate neural crest cells, derived from the neural folds, generate a variety of tissues, such as cartilage, ganglia, and cranial (intramembranous) bone. The chick homolog of the helix-loop-helix transcriptional regulator Id2 is expressed in cranial but not trunk neural folds and subsequently in some migrating cranial neural crest cells. Ectopic expression of Id2 with recombinant retroviruses converted ectodermal cells to a neural crest fate, demonstrating that proper regulation of Id2 is important for sustaining epidermal traits. In addition, overexpression of Id2 resulted in overgrowth and premature neurogenesis of the dorsal neural tube. These results suggest that Id2 may allocate ectodermal precursors into neural rather than epidermal lineages.

Neural crest cells follow migratory pathways and generate final cell types in accordance with their original rostrocaudal position along the axis (1, 2). Although both cranial and trunk neural crest cells can form melanocytes, glia, sensory neurons, and autonomic neurons (3, 4), only cranial neural crest cells have the ability to form cartilage and bone (2, 5). In screening for transcripts that are selectively expressed in cranial but not trunk neural folds (6), we isolated the chick homolog of Id2 (7) (Fig. 1, A and B). Id proteins (inhibitors of DNA binding) are negative regulators of basic helix-loop-helix (bHLH) transcription factors (7–10) that are involved in developmental processes such as myogenesis (9, 11–13), neurogenesis (14, 15), bone morphogenesis (16), lymphopoiesis (17), hematopoiesis (18), myeloid differentiation (19), and cell growth (20–22). We show that Id2 directs

ectodermal precursor toward neural crest and neurogenic fates.

In situ hybridization revealed Id2 transcripts in the most dorsal cranial neural fold region of the presumptive brain (Fig. 2, A and B). The caudal border of expression approximately corresponds to the midvagal region (Fig. 2, A and C) at the rhombomere 7/8 boundary and is maintained beyond stage 17. As neural crest cells migrated out of the neural tube, Id2 was expressed by a subpopulation of migrating cranial neural crest cells at the midbrain level (Fig. 2D). Transverse sections show Id2 mRNA in recently emigrated neural crest cells as they move toward the branchial arches (Fig. 2E). At later stages, Id2 was expressed in the region of forming cranial ganglia, such as the ciliary and trigeminal ganglia. Within the neural tube, expression became restricted to the alar plate in stage 28 embryos. In addition to expression in cranial neural fold derivatives, Id2 was expressed in the somites and subsequently in vertebral cartilage.

We explored the functional importance of Id2 in vivo by overexpressing it in the chick embryo using retrovirally mediated gene transfer with RCASBP (B) virus (replication-competent avian leukemia virus LTR splice acceptor Bryan polymerase, subgroup B envelope

B. J. Martinsen, Division of Biology, Beckman Institute 139-74, California Institute of Technology, Pasadena, CA 91125, USA, and Department of Developmental and Cell Biology, University of California, Irvine, CA 92717, USA. M. Bronner-Fraser, Division of Biology, Beckman Institute 139-74, California Institute of Technology, Pasadena, CA 91125, USA.

*To whom correspondence should be addressed. E-mail: mbronner@caltech.edu

REPORTS

genes) (23–26). Id2-expressing retrovirus (either untagged or myc-tagged) was applied to the surface ectoderm (including both ectoderm and open neural plate) of embryos ranging in age from Hamburger-Hamilton (HH) (27) stages 5 to 6 (head process stage) to HH stage 11 (12 somite stage); some embryos also received a subectodermal injection of virus into the underlying mesenchyme. Near ubiquitous expression of the retroviral gene product was observed in embryonic cells examined 1 to 3 days after infection, as assayed by staining either with antibodies to the viral protein p27 (Fig. 2F) or with the myc tag (Fig. 2, G and H).

Profound abnormalities were observed in the neural tube at the levels of the forebrain, midbrain, and hindbrain in embryos analyzed 1 to 9 days after infection. For viral infections performed at the youngest stages (HH stages 5 to 8), the ectoderm directly overlying the neural tube was absent, apparently converted to a neural crest phenotype. The normally cuboidal epithelium of the dorsal ectoderm was replaced by mesenchymal cells that express the neural crest marker, HNK-1 (Fig. 3, B and C). In contrast, embryos infected with a control virus (encoding Id2 in the antisense orientation) displayed the normal pattern of HNK-1 (Fig. 3A) and Slug (Fig. 3I) immunoreactivity, with neural crest cells clearing the dorsal surface of the neural tube by 1 day after infection. To confirm that the ectopic HNK-1-reactive cells were derived from the ectoderm, we labeled the surface ectoderm with the lipophilic dye 1,1'-dioctadecyl-3,3,3',3'-tetramethylindocarbocyanine perchlorate (DiI) after neural tube closure (28). Retrovirus was applied at the 1 to 4 somite stage followed by DiI labeling of the ectoderm after neural tube closure (~11 somite stage). In control embryos, this DiI application resulted in labeling of the surface ectoderm and a small population of invaginating placodal cells (Fig. 3D) but not of neural crest cells. In embryos infected with Id2-expressing virus, ectodermal cells close to the neural tube already appeared multilayered by the time of DiI application (11 somite stage); some DiI-labeled ectodermal cells expressed the HNK-1 epitope as early as the 14 somite stage (Fig. 3, E and F). By 1 day after infection, there was a marked overgrowth of the DiI-labeled ectoderm with numerous DiI-labeled cells in the lateral ectoderm undergoing extensive overgrowth, becoming multilayered and HNK-1 immunoreactive (Fig. 3, G and H). These results demonstrate that ectopic Id2 expression converts the DiI-labeled surface ectoderm to a neural crest phenotype. The ectoderm-to-neural crest conversion was observed in embryos infected with retrovirus before HH stage 8 (5 somite stage) and markedly declined thereafter (Fig. 3K). As it takes about 15 to 18 hours after infection to achieve high levels of ectopic protein expression (26), the time of competence to convert ectoderm to neural crest

appears to decline by HH stage 11 (13 to 14 somite stage).

Another phenotype observed with infec-

tions performed between HH stages 5 and 11 was overgrowth of the dorsal neural tube and the presence of ectopic masses of cells dorsal

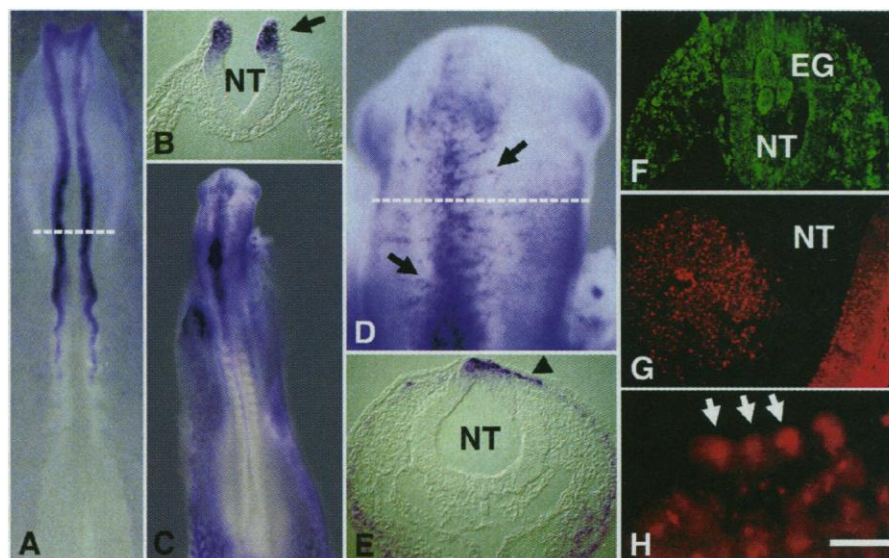
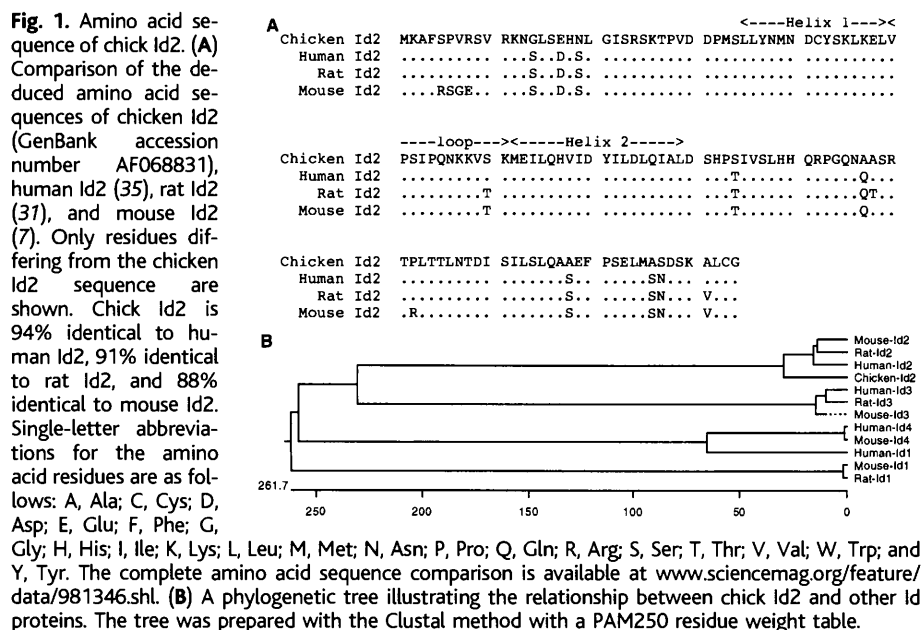


Fig. 2. Expression pattern of chick Id2, which is selectively expressed in the cranial neural folds and neural crest. (A) Whole-mount in situ hybridization of a 5 somite stage embryo reveals that Id2 is expressed in the cranial neural folds, with the caudal limit of expression in the caudal hindbrain. (B) In a transverse section of the embryo shown in (A), at the level of the dashed line, Id2-expressing cells (arrow) are within the cranial neural folds. NT, neural tube. (C) By the 11 somite stage, Id2 is expressed in the neural tube and in subpopulations of migrating neural crest cells. The caudal limit of expression remains in the caudal hindbrain. The dark spot of asymmetric expression on the left side of the embryo is in the splanchnopleure, in the region of foregut closure just caudal to the heart. (D) Higher magnification of (C) shows subpopulations of Id2-expressing neural crest cells (arrows) migrating from the neural tube. (E) In a transverse section of the embryo shown in (C) and (D) at the level of the dashed line, Id2-expressing cells appear to migrate away (arrowhead) from the neural tube and into the branchial arches. (F) After retrovirally mediated overexpression of chick Id2 in early embryos, staining with an antibody to the viral protein p27 reveals near uniform viral expression in a transverse section through an embryo injected at the 1 somite stage and fixed 1 day later. Note the ectopic ganglion (EG)-like aggregate of cells within the neural tube. (G and H) A 3-day embryo stained with antibody to myc after retroviral infection of myc-tagged Id2 reveals nuclear Id2 expression in cells within the lumen of the neural tube at low (G) and high (H) magnification; arrows in (H) indicate myc-tagged nuclei. Scale bar, 250 μ m in (A), 150 μ m in (B), 650 μ m in (C), 130 μ m in (D), 100 μ m in (E) and (F), 120 μ m in (G), and 20 μ m in (H).

REPORTS

to or within the cranial neural tube (Figs. 2, F and G, and 3, B and J). Large ganglionlike aggregates, which contained numerous neurofilament-immunoreactive cells (Fig. 3B), were observed within the lumen of the neural tube in embryos infected with either myc-Id2 or untagged Id2 virus. In embryos fixed between 2 and 9 days after infection, ectopic masses were found within the cerebellum and brain vesicles, which protruded from the cranium lacking dorsal ectoderm (Fig. 3L). In contrast, the majority of embryos infected with control virus displayed no obvious abnormalities (Fig. 3M).

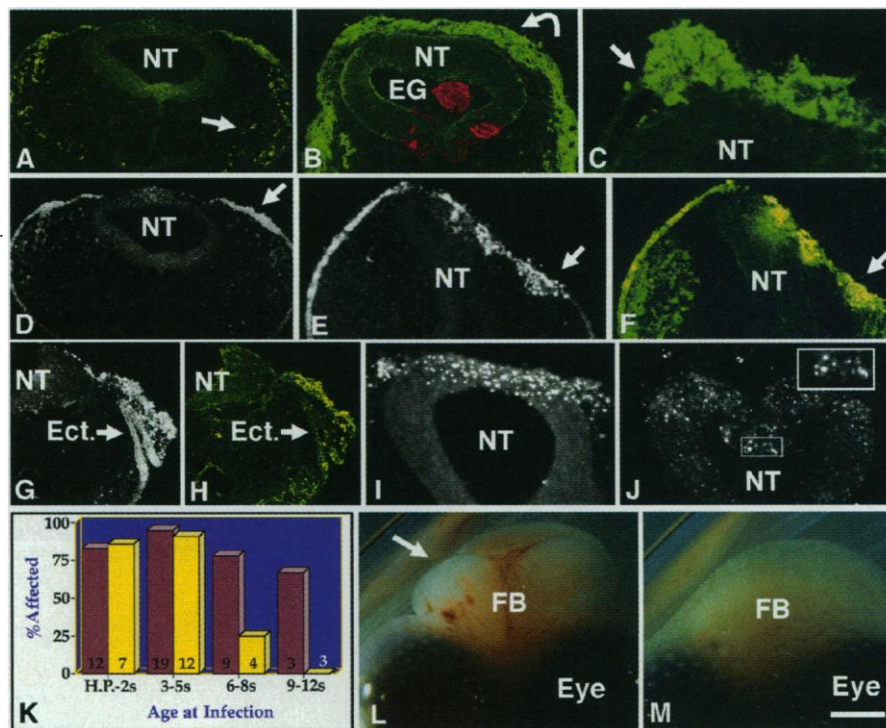
When retroviral constructs were injected into the cranial mesenchyme instead of the neural tube, all tissues except the neural tube expressed the viral protein p27 or the myc tag (or both), suggesting that the virus does not cross the basal lamina of the neural tube. No

defects were observed in these embryos. Thus, ectopic expression of Id2 appears only to affect ectodermally derived cells at or near the ectoderm-neuroectoderm border, where Id2 is normally expressed. No morphological abnormalities were observed in the trunk of infected embryos. Because Id2 heterodimerizes with other HLH transcription factors, the ability to detect a phenotype may be directly related to the availability of the appropriate partner.

Here, we have shown that the HLH transcriptional regulator Id2 directs ectodermal precursors into neural instead of epidermal lineages. In the chick, Id2 is differentially expressed in the cranial, but not trunk, neural folds. Consistent with the expression of Id2 in the cranial neural folds, Id proteins are often associated with sites of active epithelial-mesenchymal transitions (29). Overex-

pression of Id2 results in an epidermal-to-neural crest conversion, suggesting that the bHLH partner to Id2 may promote epidermalization. Because individual neural fold cells can become epidermis, neural crest, or neural tube cells (30), the expression of Id2 in the neural folds may maintain a balance between these fates such that the appropriate proportion of cells enters the neural crest and neural tube lineages. Cranial ganglia are derived from both the neural crest and the ectodermal placodes; furthermore, both placode- and neural crest-derived cells express the HNK-1 epitope. Therefore, we cannot rule out the possibility that overexpression of Id2 drives some ectodermal cells into a placodal fate; however, Id2 is not normally expressed in the placodes. The ectopic, ganglionlike aggregates observed after Id2 overexpression suggest an effect on promotion of neurogenesis,

Fig. 3. Retrovirally mediated overexpression of chick Id2 in early embryos. (A) An embryo infected with control virus encoding antisense Id2 displays the normal pattern of HNK-1 immunoreactivity, with neural crest cells (arrow) migrating away from and clearing the dorsal surface of the neural tube. (B) A transverse section through an embryo injected with Id2 retrovirus at the 1 somite stage, fixed after 1 day, and stained with HNK-1 antibody (green) and neurofilament antibody (red). The ectoderm overlying the neural tube was absent and was replaced by large masses of HNK-1-positive cells (curved arrow). A large aggregate of neurofilament-positive cells appeared to form an ectopic ganglion within the neural tube. (C) Another section through the embryo in (B), showing that the cuboidal epithelium of the ectoderm ends and meets (arrow) mesenchymal HNK-1-immunoreactive cells. (D) The surface ectoderm of the embryo in (A) was labeled with the lipophilic dye Dil after neural tube closure, resulting in labeled cells (arrow) in the surface ectoderm and a small population of invaginating placodal cells. (E and F) Dil labeling (E) and HNK-1 immunoreactivity (F) of an embryo infected with Id2-expressing virus showing a marked overgrowth of the ectoderm as early as 5 hours after Dil labeling (14 somite stage); some of the Dil-labeled cells [arrow in (E)] are also HNK-1-positive [arrow in (F)]. (G and H) Dil labeling (G) and HNK-1 immunoreactivity (H) of an embryo 1 day after being infected with Id2-expressing virus; there was a marked over growth of the ectoderm (Ect.), some of which is HNK-1-positive. (I) Slug antibody staining of an embryo 1 day after infection of control virus shows expression in the dorsal neural tube and migrating neural crest cells. (J) Slug antibody staining of an embryo 1 day after infection of Id2 retrovirus shows that a mass of Slug-expressing cells has invaginated into the neural tube (insets). After 1 day, abnormal ectoderm neural tube (or both) phenotypes were observed in 36 of 39 embryos infected with myc-Id2 virus and 9 of 12 embryos with untagged Id2, confirming that the myc tag did not interfere with function of the Id2 construct; 2 of 16 control embryos had abnormalities in the neural tube (typical of the background level of defects observed in noninfected embryos). (K) Conversion of the embryonic ectoderm into neural crest and formation of ectopic ganglia after infection with Id2 retrovirus. Yellow graph shows the percentage of embryos in which the surface ectoderm over the neural tube has been converted into HNK-1-positive cells as a function of stage of infection. Embryos were analyzed 1 day after infection. Between head process (H.P.) and 5 somite stage, 89% of embryos exhibited an ectoderm-to-neural conversion. Between the 6 and 8



somite stages, this phenotype rapidly declined. Given that protein expression takes 15 to 18 hours (24, 26), this decline suggests that the ectoderm loses the ability to be converted to neural crest cells at the 14 somite stage. Maroon graph shows the percentage of embryos with aggregates of ectopic neural crest-like ganglia within or above the dorsal neural tube as a function of stage of infection. Similar phenotypes were observed for infections performed between head fold and the 12 somite stage, the last stage examined. The total number of embryos is shown within each bar. (L) An embryo injected with Id2 retrovirus at the 4 somite stage and allowed to develop for 9 days. The ectoderm over the dorsal neural tube (arrow) was absent, and the forebrain (FB) was not contained within the cranium, perhaps because of overgrowth of the neural tissue. (M) A control embryo injected with antisense Id2 retrovirus at the 4 somite stage and fixed after 9 days. The ectoderm over the neural tube is continuous. In embryos fixed between 2 and 9 days after infection, abnormalities were observed in 8 of 8 Id2-infected embryos and in 0 of 6 control embryos. Scale bars, 90 μ m in (A), (D), (G), and (H); 80 μ m in (B); 40 μ m in (C); 70 μ m in (E) and (F); 50 μ m in (I) and (J); and 2.5 mm in (K) and (L).

consistent with studies demonstrating Id expression in dividing neuroblasts (15, 31), presumptive interneurons, and motor neurons in the developing spinal cord (15). In *Drosophila melanogaster*, the Id homolog extramacrochaete regulates sensory organ patterning in the adult fly epidermis by negatively regulating the bHLH proteins achaete and scute (32, 33) in a dose-dependent manner (33, 34). In vertebrates, our results demonstrate that Id2 plays stage-dependent roles in ectodermal development, likely depending on the presence of other interacting bHLH molecules. Thus, Id2 heterodimers may maintain the balance between differentiation and proliferation in neural crest and ectodermal precursors.

References and Notes

1. N. Le Douarin, *The Neural Crest*, vol. 12 of *Developmental and Cell Biology Series* (Cambridge Univ. Press, Cambridge, 1982).
2. D. M. Noden, *Dev. Biol.* **42**, 106 (1975).
3. N. M. Le Douarin and M. A. Teillet, *ibid.* **41**, 162 (1974).
4. G. G. Leblanc, M. L. Epstein, M. E. Bronner-Fraser, *ibid.* **137**, 318 (1990).
5. H. Nakamura and C. S. Ayer-le Lievre, *J. Embryol. Exp. Morphol.* **70**, 1 (1982).
6. RNA was isolated from the presumptive midbrain cranial neural folds (four to six somites) and from dispase-isolated trunk (16 to 22 somites) neural tubes (spanning the last three somites up to Hensen's node) of White Leghorn chicken embryos, with RNazol B (Tel-Test). The resulting pools of RNA were compared by Differential Display (Display Systems). Subsequently, one differentially displayed band was used for whole-mount in situ hybridization and for a 12 to 15 HH stage chick embryo library screen.
7. X. H. Sun, N. G. Copeland, N. A. Jenkins, D. Baltimore, *Mol. Cell. Biol.* **11**, 5603 (1991).
8. S. Sawai and J. A. Campos-Ortega, *Mech. Dev.* **65**, 175 (1997).
9. R. Benezra, R. L. Davis, D. Lockshon, D. L. Turner, H. Weintraub, *Cell* **61**, 49 (1990).
10. H. Zhang, S. Reynaud, M. Kloc, L. D. Etkin, G. Spohr, *Mech. Dev.* **50**, 119 (1995).
11. Y. Jen, H. Weintraub, R. Benezra, *Genes Dev.* **6**, 1466 (1992).
12. T. J. Brennan, D. G. Edmondson, L. Li, E. N. Olson, *Proc. Natl. Acad. Sci. U.S.A.* **88**, 3822 (1991).
13. L. A. Neuhoff and B. Wold, *Cell* **74**, 1033 (1993).
14. T. Neuman et al., *Dev. Biol.* **160**, 186 (1993).
15. Y. Jen, K. Manova, R. Benezra, *Dev. Dyn.* **208**, 92 (1997).
16. T. Ogata, J. M. Wozney, R. Benezra, M. Noda, *Proc. Natl. Acad. Sci. U.S.A.* **90**, 9219 (1993).
17. R. B. Wilson et al., *Mol. Cell. Biol.* **11**, 6185 (1991).
18. G. Condorelli et al., *Blood* **86**, 164 (1995).
19. A. Ishiguro et al., *ibid.* **87**, 5225 (1996).
20. B. A. Christy et al., *Proc. Natl. Acad. Sci. U.S.A.* **88**, 1815 (1991).
21. A. Iavarone, P. Garg, A. Lasorella, J. Hsu, M. A. Israel, *Genes Dev.* **8**, 1270 (1994).
22. W. Shoji, T. Inoue, T. Yamamoto, M. Obinata, *J. Biol. Chem.* **270**, 24818 (1995).
23. Vectors with or without a myc tag were made with VENT DNA polymerase. A cDNA fragment of the chick Id2 coding region was amplified with Eco R1 and Ava 1-Stu 1 primer linkers, and a cDNA fragment for the non-myc-tagged vector was amplified with Nco 1 and Ava 1-Stu 1 primer linkers. Between all cloning steps, the cDNA fragments were purified with a GeneClean Kit from BRL. The amplified chick Id2 coding region used to make the myc-tagged RCASBP (B) vector was cloned into the Eco R1 and Stu 1 sites of a CS2 + MT (myc tag) vector, cut with Nco 1 and Ava 1, cloned into a SLAX-13 shuttle vector at the Nco 1 and Ava 1 sites, cut with Cla 1, and cloned into

- the Cla 1 site of a RCASBP (B) vector. The non-myc-tagged vector was cloned directly into the SLAX-13 vector, bypassing the CS2 + MT (myc tag) vector. Infection of chicken embryonic line O fibroblast cells revealed expression of myc-tagged Id2 protein in the nucleus of nearly all cells by 2 days after infection, demonstrating proper expression.
24. B. C. Morgan and D. M. Fekete, in *Methods in Avian Embryology*, M. Bronner-Fraser, Ed. (Academic Press, San Diego, CA, 1996), vol. 51, pp. 186-217.
25. S. H. Hughes, J. J. Greenhouse, C. J. Petropoulos, P. Suttrave, *J. Virol.* **61**, 3004 (1987).
26. S. A. Homburger and D. M. Fekete, *Dev. Dyn.* **206**, 112 (1996).
27. V. Hamburger and H. L. Hamilton, *J. Morphol.* **88**, 49 (1951).
28. J. Sechrist, M. A. Nieto, R. T. Zamanian, M. Bronner-Fraser, *Development* **121**, 4103 (1995).
29. Y. Jen, K. Manova, R. Benezra, *Dev. Dyn.* **207**, 235 (1996).

30. M. A. Selleck and M. Bronner-Fraser, *Development* **121**, 525 (1995).
31. Y. Nagata, W. Shoji, M. Obinata, K. Todokoro, *Biochem. Biophys. Res. Commun.* **207**, 916 (1995).
32. J. Garrell and J. Modolell, *Cell* **61**, 39 (1990).
33. H. M. Ellis, D. R. Spann, J. W. Posakony, *ibid.*, p. 27.
34. J. Botas, J. Moscoso del Prado, A. Garcia-Bellido, *EMBO J.* **1**, 307 (1982).
35. E. Hara et al., *Dev. Genet.* **18**, 161 (1996).
36. We thank S. Fraser, C. Baker, and M. Dickinson for critical reading of the manuscript; J. Sechrist for critical analysis of ectoderm conversion data; C. Marcelle, T. Moreno, M. Barembaum, and C. LaBonne for advice on molecular biology protocols; and K. Min and J. Neri for cryostat sectioning. We are grateful to S. Bryant and D. Gardiner for the stage 13 to 24 chick embryo library. Supported by U.S. Public Health Service grants NS34671 and NS36585.

16 March 1998; accepted 1 July 1998

Crystal Structure of Hemolin: A Horseshoe Shape with Implications for Homophilic Adhesion

Xiao-Dong Su,* Louis N. Gastinel,† Daniel E. Vaughn,‡
Ingrid Faye, Pak Poon, Pamela J. Bjorkman§

Hemolin, an insect immunoglobulin superfamily member, is a lipopolysaccharide-binding immune protein induced during bacterial infection. The 3.1 angstrom crystal structure reveals a bound phosphate and patches of positive charge, which may represent the lipopolysaccharide binding site, and a new and unexpected arrangement of four immunoglobulin-like domains forming a horseshoe. Sequence analysis and analytical ultracentrifugation suggest that the domain arrangement is a feature of the L1 family of neural cell adhesion molecules related to hemolin. These results are relevant to interpretation of human L1 mutations in neurological diseases and suggest a domain swapping model for how L1 family proteins mediate homophilic adhesion.

Insects have developed highly efficient innate forms of immunity against invading microorganisms such as bacteria and fungi (1). In the giant silkworm *Hyalophora cecropia* and the tobacco hornworm *Manduca sexta*, many

proteins are up-regulated in larvae or pupae upon bacterial infection. Hemolin is present in low amounts in the hemolymph of naïve insects, but is highly induced upon bacterial infection, and is assumed to be an integral component of the insect immune response (2).

Hemolin is a member of the immunoglobulin superfamily (IgSF), containing four Ig-like domains (3). It shares significant sequence similarity with the first four domains of the IgSF portion of transmembrane cell adhesion molecules (CAMs) of the L1 family, whose extracellular regions consist of six IgSF domains followed by five fibronectin III repeats (4) [~38% amino acid sequence identity between hemolin and the four NH₂-terminal IgSF domains of neuroglian (3), the insect ortholog of mammalian L1]. L1 family members mediate homophilic and heterophilic adhesion events that facilitate neurite outgrowth and fasciculation. Mutations in the human L1 gene are found in a variety of neurological disorders (4, 5).

X.-D. Su, L. N. Gastinel, P. J. Bjorkman, Division of Biology 156-29 and Howard Hughes Medical Institute, California Institute of Technology, Pasadena, CA 91125, USA. D. E. Vaughn, Division of Biology 156-29, California Institute of Technology, Pasadena, CA 91125, USA. I. Faye, Department of Genetics, Stockholm University, S-106 91 Stockholm, Sweden. P. Poon, Department of Chemistry and Biochemistry, University of California at Los Angeles, Los Angeles, CA 90095, USA.

*Present address: Department of Molecular Biophysics, Center for Chemistry and Chemical Engineering, Post Office Box 124, Lund University, S-221 00 Lund, Sweden.

†Present address: AFMB, CNRS UPR 9039, 31 Chemin Joseph Aiguier, 13402 Marseille Cedex 20, France.

‡Present address: Cold Spring Harbor Laboratory, 1 Bungtown Road, Cold Spring Harbor, NY 11724, USA.

§To whom correspondence should be addressed. E-mail: bjorkman@cco.caltech.edu